Measurement of Si 311 defect properties using x-ray scattering

K. Nordlund[a)]
Accelerator Laboratory, P.O. Box 43, University of Helsinki, Helsinki FIN-00014, Finland

T. H. Metzger, A. Malachias, and L. Capello
European Synchrotron Radiation Facility (ESRF), BP220, F-38043, Grenoble Cedex, France

P. Calvo and A. Claverie
Groupe nanomateriaux, Centre d'Elaboration de Matériaux et d'Etudes Structurales/Centre National de la Recherche Scientifique (CEMES/CNRS), 29 Rue Jeanne Marvig, BP94347, 31055 Toulouse Cedex 4, France

F. Cristiano
Groupe Technology Micro et Nanostructures (TMN), Laboratoire d'Analyse at d'Architecture des Systèmes (LAAS/CNRS), 7 Avenue du Colonel Roche, 31077, Toulouse Cedex 4, France

The 311 defects play a crucial role in the damage healing and dopant redistribution which occurs during the annealing of an ion-beam-doped Si. Using grazing-incidence x-ray scattering we measure the type, length, and width of the 311 defects created with different annealing times. In particular, we show that measurements around (1.3 1.3 0) in reciprocal space can be used to determine all these quantities without the need for pristine reference samples. The results agree well with computer simulation predictions and transmission-electron-microscopy measurements, demonstrating that x-ray methods can be used as a nondestructive, rapid method to characterize the 311 defects. © 2005 American Institute of Physics. [DOI: 10.1063/1.2081111]

INTRODUCTION

Ion implantation is the standard method for introducing electrically active dopants into Si.[1] Although the method has several advantages, one drawback is that room-temperature implantation to high doses amorphizes the sample, and a subsequent high-temperature annealing stage is needed to recover the crystalline structure. Several types of interstitial-like extended defects play a central role in the kinetics of annealing.[2] The vast majority of these defects have to be removed in order to produce working semiconductor devices, so the properties of these defects are of great interest. The most important extended defects are the so-called 311 defects, stacking faults, and perfect dislocation loops.

All of these extended defects can be detected using transmission electron microscopy (TEM), but it would be beneficial to have complementary, nondestructive means to detect the same defects. The only alternative method which can detect all kinds of extended defects is the diffuse x-ray scattering (DXS). Previous experiments and theory have shown how DXS can be used to detect stacking faults and dislocation loops.[3–8] However, previous theories had not established what the DXS line shape from the third important defect type in Si, the 311 defects, would look like. Recently, Nordlund used a fully atomistic simulation model[9,10] to predict the DXS line shape from the 311 defects.[11] In the current work we use a combination of TEM and DXS analyses to confirm the theoretical prediction and show that the experiments can be used to detect not only the presence but also the type, length, and width of the 311 defects.

From previous electron microscopy and computer simu-

lations the atomic structure of the 311 defects is fairly well understood[12–14] and we only recall the central features here. The name of the defects stems from the fact that the interstitial atoms lie on planes perpendicular to the ⟨311⟩ crystal directions. However, in many cases the ⟨311⟩ planes alternate in a zigzag pattern to produce a defect where the overall plane is a ⟨100⟩ (see Fig. 1). Parisini and Bourret have convincingly shown that the main varieties of the 311 defects are the "IRD" rectilinear defect lying on the ⟨311⟩ planes and the "1HexZD" zigzag defect lying on the ⟨100⟩ planes.[12] The defects are called rodlike because they typically are mi-
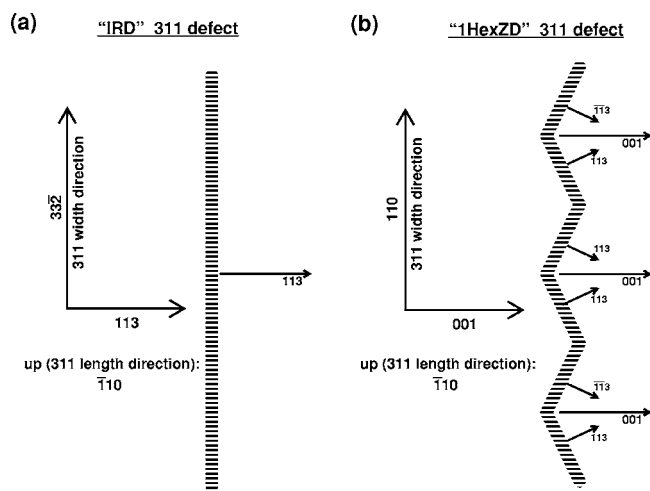

FIG. 1. Schematic illustration of the orientation of the 311 defects. The plane where the extra atoms lie is indicated by thick, dashed lines. The vectors and numbers show crystal directions and their Miller indices. The defect names and the orientation information is from Ref. 12. (a) IRD defect, (b) 1HexZD defect.

a)Electronic mail: kai.nordlund@helsinki.f1

98, 073529-1

crometers long, but only 1-100 nm wide. The thickness is limited to a couple of atomic layers since otherwise the core energy of the defect plane becomes prohibitively large.[12]

Nordlund simulated the DXS line shape from these defects,[11] and obtained the following main results. The IRD defect is expected to have streaks emanating from Bragg peaks in the $\langle 311 \rangle$ directions, and the 1HexZD defect streaks in the $\langle 100 \rangle$. These streaks are similar to the ones due to stacking faults, which have been experimentally observed to emanate in the $\langle 111 \rangle$ directions from Bragg peaks.[6,7,15]

The simulations further predicted that the IRD defects produce strong scattering around (1.35 1.35 0) in reciprocal space, and the 1HexZD defect around (1.25 1.25 0) in reciprocal space. Scattering in this region has previously been observed in electron-diffraction experiments, but no fine structure was resolved.[13] This region of reciprocal space does not of course contain any Bragg reflection. But the 311 defect can be considered to be a single layer of hexagonal Si, and it turns out that the (0002) Bragg peak of a hexagonal Si can be visible, close to (1.3 1.3 0) in a cubic Si if the 311 defects exist in the sample.[12,13] Note that due to this, the x-ray scattering from the 311 defects at (1.3 1.3 0) is not diffuse scattering from the long-range strain field but from the defect core itself.

The simulations also showed that the width of the 311 defects is inversely proportional to the streak width in the $[33\bar{2}]$ direction (IRD) or the $[110]$ direction (1HexZD), and the length of the 311 defects is inversely proportional to the streak width in the $[\bar{1}10]$ direction.

The simulations carried out in Ref. 11 were based on the Tersoff interatomic potential.[16] To rule out model dependencies, as part of the current work, we repeated a few calculations with the Stillinger-Weber potential.[17] We found that the diffuse-scattering intensity values differ only by a few percent, and most importantly for the current work the line shapes are practically identical.

EXPERIMENTAL PROCEDURE

Sample preparation

The samples were prepared under conditions known to produce a high fraction of the 311 defects compared with any other defect variety. Si$^+$ was implanted at 100 keV with a nominal dose of 2×10^{14} atoms/cm^2 into a silicon (100) wafer. Following this implant, pieces of the wafer were annealed at 800 °C for increasing times ranging from 1 to 45 min under nitrogen. Samples for plan-view and cross-sectional electron microscopies were prepared following the standard technique involving mechanical thinning and ion milling for electron transparency.

TEM measurements

To ensure that the current samples do contain the expected high concentration of the 311 defects, parts of the samples were characterized using TEM. The TEM images used for the statistical measurements of the lengths and surface densities of the {311} defects were obtained on the plan-view specimen under weak-beam-dark-field (WBDF) condi-

tions. These WBDF images were taken along the [113] zone axis (ZA) with **g**=422. Only these imaging conditions allow the identification and the measurement of all the 12 variants of these defects on the same image. Details of this new method are given elsewhere.[18] The size distributions and densities which are obtained are thus very accurate and can be used as a reliable data bank against which x-ray measurements can be compared. On the other hand, depth distributions of defects were extracted from WBDF images of the cross-sectional specimen (with [110] ZA and **g**=220) taken from relatively thick ($\sim$500 nm) and flat regions of the sample.[19] It has to be noted that ensuring a high statistics, i.e., measuring a very large number of defects, is a prerequisite condition for evidencing the strong asymmetry of the length distribution of these defects.[18]

X-ray measurements

An x-ray analysis was carried out at beam line ID01 of the European Synchrotron Radiation Facility. Since cross-sectional TEM is a destructive technique, the x-ray characterization was performed on pieces of the sample adjacent to those used in the TEM.

Since the defects are expected to be located close to the surface, the x rays are made near surface sensitive by performing the scattering experiment at grazing angles for incidence and exit, close to the critical angle α_c of the total external reflection. Under these conditions only a small cross section of the incident beam of about 0.1 mm is accepted by the sample. Together with the expected weak-defect-induced DXS intensity, the use of highly brilliant x rays as provided at station ID01 is mandatory. To increase the flux within a tolerable small divergence, the incident beam was focused horizontally and vertically at the sample position to a size of 0.2×0.2 mm^2, illuminating the sample with about 10^{12} photons/s. The energy of the x rays was set to 8.00 keV. For efficient data collection the scattered intensity was recorded by a linear position-sensitive detector placed perpendicular to the sample surface, thus collecting intensity along the [001] surface normal. For details of the technique see Sztucki *et al.*.[15] Radial and angular scans, parallel and perpendicular to the scattering vector, respectively, have been performed close to (1.3 1.3 0) and the (220) Si Bragg peak. At the (1.3 1.3 0) position, the 311 defects are expected to give the main contribution to the scattering,[11] except for some structureless thermal diffuse and Compton scattering. Close to the (220) the defect-induced DXS is competing mainly with thermal diffuse scattering, and a clear interpretation of the DXS is only possible after a pristine Si sample is measured under the same conditions to evaluate the background scattering. Since untreated Si crystals have not been measured, the data analysis in this paper is focused mainly on the region close to (1.3 1.3 0). The measurements in angular space are transformed into reciprocal space maps in the plane spanned by the [110], [001] and the [1$\bar{1}$0], [001] directions for the radial and angular measurements, respectively. The linewidth of the intensity humps is obtained from the total signal of the position-sensitive detector (exit-angle

TABLE I. Samples used and results of the measurements. The samples were implanted with 100 keV 2×10^{14} Si ions/cm² and subsequently annealed at 800 °C to the times indicated. The uncertainties are 1σ errors of the average. The defect lengths are along the $[\bar{1}10]$ direction and the widths are along the $[110]$ direction.

Label	Annealing time (min)	$\bar{l}$, TEM (Å)	$\bar{l}$, DXS (Å)	$\bar{w}$, DXS (Å)
K1	1	114±4	194±2	30.8±0.4
K2	5	334±23	827±8	32.4±0.1
K3	10	502±33	1134±7	38.2±0.2
K4	30	1105±74	1686±16	42.1±0.2
K5	45	1670±120	1770±53	48.5±0.5

integrated intensity). In all cases resolution effects due to the finite-beam divergence can totally be neglected.

RESULTS

The reference TEM results on the defect length $\bar{l}$ are shown in Table I.

The x-ray measurements were carried out in two regions of reciprocal space: around the (220) Bragg peak and around (1.3 1.3 0) in reciprocal space. Because of the glancing-incidence geometry used, the measurements were restricted to positive values of l in (hkl).

The streak features described above offer a straightforward way to determine whether the 311 defects in the sample are mainly IRD-like or zigzag (1HexZD)-like. For IRD, the measurement along $[110]$ slightly above the central spot in the $[110]$, $[001]$ plane should give rise to two separate streaks in the $[\bar{1}\bar{1}3]$ and $[113]$ directions. The splitting is expected both for the (220) and (1.25 1.25 0) peaks. On the other hand, for 1HexZD there should only be one streak in the $[001]$ direction, both at the (220) and (1.3 1.3 0), possibly surrounded by much weaker side maxima giving the repetition length of the zigzag pattern.[11]

The measurements around (220) gave a strong and wide streak extending in the $[001]$ direction, where no clearly resolved structure could be discerned (see Fig. 2). Such an
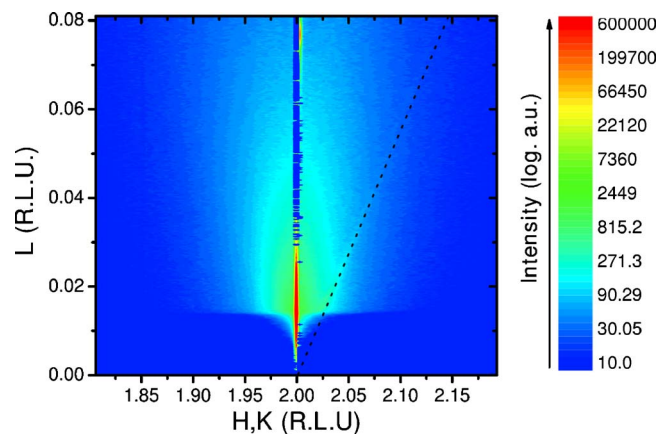

FIG. 2. (Color online) Two-dimensional map of the scattering intensity around (220) in reciprocal space for sample K4. R.L.U. stands for reciprocal lattice units. The strong scattering which extends in the L ([001]) direction in reciprocal space is the crystal truncation rod. The streak in the 111 direction is highlighted with a black dashed line.

intensity distribution is typical for thermal diffuse scattering, and any possible signal from the 311 defects is overshadowed by this background. The measurements around (220) do, however, show a clear streak in the $[111]$ direction, which has previously been shown to correspond to scattering from stacking faults.[6] This streak was not observed in the samples annealed for shorter times, which indicates that during the longer-time annealings a small fraction of the 311 defects have evolved into stacking faults. This is the behavior expected based on the recently obtained good understanding of the kinetics of extended defects in Si.[20]

The measurements around (1.3 1.3 0) in reciprocal space did give a clear signal from the defects. Moreover, since this region is far from any Bragg peak, the background which does exist is fairly flat.

To ensure that the signal received is indeed from the defects of interest, the scans were also performed at incident angles α_i less than α_c. In this way, the beam only penetrates the top few nanometres of the sample. Since the TEM measurements show that all the 311 defects are at least about 100 nm deep in the samples, this measurement should give no signal due to the defect. As expected, only a flat background signal was observed for $\alpha_i < \alpha_c$ (see Fig. 5).

When the incident angle was raised above the critical angle, i.e., when the x-ray beam also probed the inside of the sample, a clear streak raising above the background was observed (see Figs. 3 and 5). Note that the maximum is almost exactly at $h=1.25$ (Ref. 21) (not $h=1.35$ as expected for IRD defects) and that the streak is not split at higher values of l. The same was true for all the samples measured. Combined with the simulation results described above, these observations indicate that the 311 defects are predominantly of the 1HexZD variety.

There are no weaker side maxima visible in the data. The likely explanation to this comes from the fact that the side maxima measure the repetition distance of the zigzag pattern in the defect. In the simulations in Ref. 11 only one defect was simulated at the time, so the side maxima were well localized. The current experiments, however, average over a large number of defects, and the repetition distance is likely to vary. Hence the sum of the side maxima becomes much broadened, making them hard to distinguish from the background (note that the background is now roughly 1/3 of the signal, while the side maxima reported in Ref. 11 are approximately one order of magnitude weaker than the main one). Hence experiments with a better statistics or elsewhere in reciprocal space would be needed to resolve the fine structure around the main streak, and this would definitely resolve whether the defects are of the 1HexZD or IRD variety.

Also interesting is that a comparison of in Figs. 3(a) and 3(b) clearly shows that the streak in (b) is much narrower than the one in (a). Due to the relation between the streak width and the defect size described in the Introduction, the difference between the two figures shows that the defects are much longer than they are wide. This is as expected for the typical rodlike shape of the defects.

Determining the streak width allows us to also determine their average length and width quantitatively. This is as expected from the basic scattering theory, but was also proven
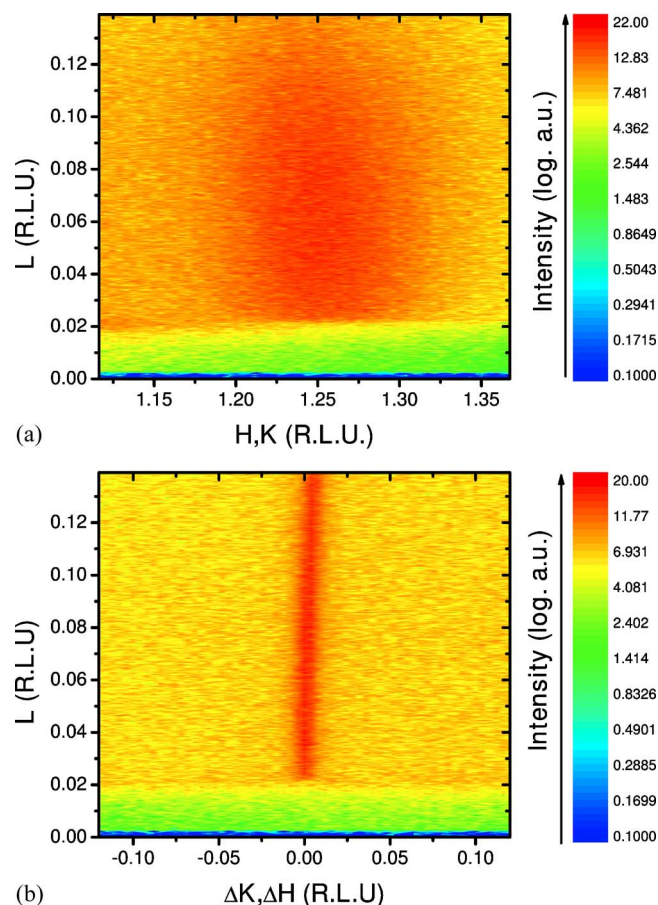
FIG. 3. (Color online) X-ray scattering map around (1.3 1.3 0) in reciprocal space for sample K3. (a) Measurement in the plane spanned by the [110],[001] directions in reciprocal space. The width of this streak is inversely proportional to the width of the defect along [110] in direct space.[11] (b) Measurements in the plane spanned by the [$\bar{1}$10], [110] direction in reciprocal space. The width of this streak is inversely proportional to the length of the defect along [$\bar{1}$10] in direct space.[11]

FIG. 4. X-ray scattering intensity from all samples measured near (1.3 1.3 0) in reciprocal space. (a) Radial scans, corresponding to defect widths u; (b) angular scans, corresponding to defect lengths l. The background has been subtracted from the data, and the maxima set to the same value to illustrate the change in the streak width. The abscissa is shown in angles since the defect sizes were determined using the width in angles. Note that for all annealings longer than 1 min the streak is much narrower in the angular than in the radial direction. This shows that the 311 defects are rodlike, consistent with the general shape in which they are observed in experiments. The inset in part (a) shows a direct comparison of the streak width for the 1 min annealed sample (width of 30.8 Å) with atomistic simulations of a 30 Å wide 311 defect (Ref. 11). The simulated width is slightly broader than the experimental one due to the convolution factor σ used in the simulations.

explicitly for the current problem by the atomistic simulations in Refs. 6 and 11. From the streak width in the angular scans the defect length was determined using the equation $l = \lambda/[2\sin\theta d(\theta)]$ where θ is the location of the maximum and $d(\theta)$ is the full width at half maximum (FWHM) of the streak. Correspondingly, from the streak width in the radial scans the defect width was determined using $w = \lambda/[\cos(\theta/2)d(\theta)]$. Alternatively one could also determine the widths by direct comparison with the atomistic simulations, but this is complicated by effects of the convolution factor σ (Ref. 11 [see inset in Fig. 4(a)].

The streak widths were determined by fitting a Gaussian or Lorentzian line shape plus a linear curve describing the background to the data. The fitted data for all measured samples is shown in Fig. 4, and the fitting result for one of them is illustrated in Fig. 5.

The fitting was carried out using the Marquardt method,[22] weighting the data points with their statistical uncertainties. The FWHM of the peak was determined from the width parameter fitting result of the respective line shapes, neglecting the background terms. Both the Gaussian and Lorentzian line shapes gave comparably good fits to the peaks (within the statistical fluctuations), and the FWHM
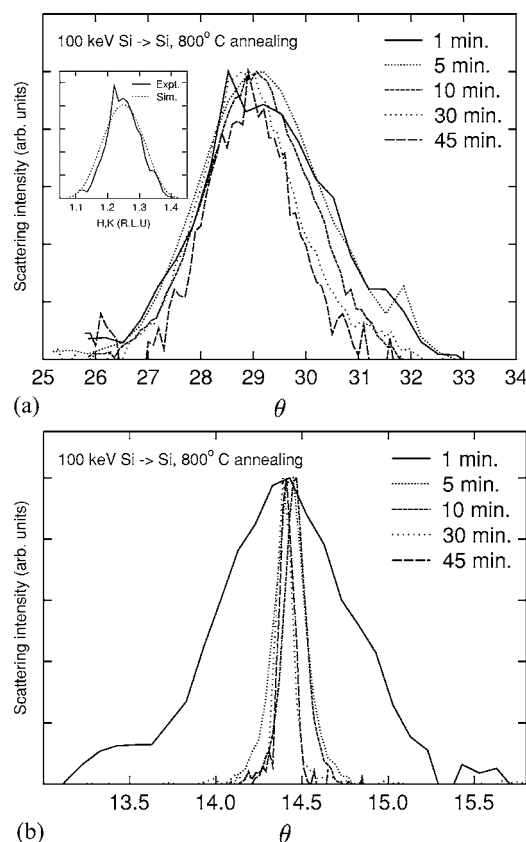
values obtained agreed in all cases within ~10%. For the remainder of the analysis we used the FWHM results obtained from the Gaussian fits.

The fitting result is illustrated for one of the samples in Fig. 5, and the obtained defect length and width values are given in Table I. The TEM and DXS values are in excellent qualitative agreement; both show that the defect lengths l steadily increase during annealing, the difference between the 1 and 45 min. annealed samples being about an order of magnitude.

The quantitative agreement is not so good, at least in part, because the DXS and TEM methods do not measure exactly the same thing. The TEM measurement was carried out on a plan-view sample and hence is an average of defect sizes at all depths. The x rays, on the other hand, attenuate with depth, and hence the DXS signal gives more weight to defects close to the surface, although in the present measurements this should be a minor effect. Unfortunately, taking the depth distribution into account in the analysis is complicated
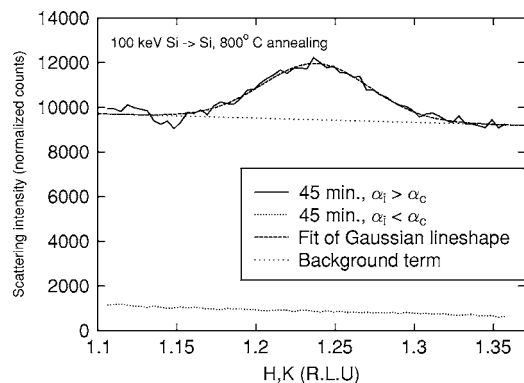
FIG. 5. X-ray scattering intensity from sample K3 measured along [110] on both sides of (1.3 1.3 0) in reciprocal space. Also shown is the intensity measured only for the near-surface region (below the critical angle for total external reflection) and the linear background subtraction term.

and beyond the scope of the present work, where the main aim is to demonstrate that the 311 defects can indeed be characterized by x rays.

The defect widths (which are hard to determine accurately in the TEM measurements) only grow weakly with annealing time, from about 31 to 48Å. This clearly shows that the 311 defects grow predominantly in their length direction.

DISCUSSION AND CONCLUSIONS

Our results, which indicate that the majority of the 311 defects are of the 1HexZD variety, are well in line with those of previous works which indicate that an ion-implanted Si predominantly has this variety of the 311 defects.[12,13] Also the widths we observe are well in line with the previously reported values of about 4–8 nm under similar implantation conditions.[23,24]

The use of the region around (1.3 1.3 0) in reciprocal space to characterize the 311 defects offers many advantages. As described above, the background is very low and featureless in this region of reciprocal space. Moreover, none of the other common extended defects (small clusters, stacking faults, and perfect dislocation loops) has any particularly strong signal in this region of reciprocal space.[3,6,10,25] This means that even in samples with a mixture of the 311 and other defects, one can expect to be able to characterize the 311 defects without a signal overlap with other defect types. These issues will be explored further in a future work.

In conclusion, we have shown that x-ray methods can be used as a nondestructive, rapid method to detect the 311 defects and that it allows for determining both the length and the width of the defects.

ACKNOWLEDGMENTS

[1]J. W. Mayer and S. S. Lau, *Electronic Materials Science For Integrated Circuits in Si and GaAs* (MacMillan, New York, 1990).
[2]E. Chason *et al.*, J. Appl. Phys. **81**, 6513 (1997), and references therein.
[3]P. Ehrhart, H. Trinkaus, and B. C. Larson, Phys. Rev. B **25**, 834 (1982).
[4]S. Grotehans, G. Wallner, E. Burkel, H. Metzger, J. Peisl, and H. Wagner, Phys. Rev. B **39**, 8450 (1989).
[5]P. Ehrhart, J. Nucl. Mater. **216**, 170 (1994).
[6]K. Nordlund, U. Beck, T. H. Metzger, and J. R. Patel, Appl. Phys. Lett. **76**, 846 (2000).
[7]D. Luebbert, J. Arthur, M. Sztucki, T. H. Metzger, P. B. Griffin, and J. R. Patel, Appl. Phys. Lett. **81**, 3167 (2002).
[8]M. A. Kirk, R. S. Davidson, M. L. Jenkins, and R. D. Twesten, Philos. Mag. **85**, 497 (2004).
[9]K. Nordlund, P. Partyka, and R. S. Averback, Mater. Res. Soc. Symp. Proc. **469**, 199 (1997).
[10]K. Nordlund, P. Partyka, R. S. Averback, I. K. Robinson, and P. Ehrhart, J. Appl. Phys. **88**, 2278 (2000).
[11]K. Nordlund, J. Appl. Phys. **91**, 2978 (2002).
[12]A. Parisini and A. Bourret, Philos. Mag. A **67**, 605 (1992).
[13]A. Bourret, Inst. Phys. Conf. Ser., **87**, 39 (1987).
[14]S. Takeda, Jpn. J. Appl. Phys., Part 2 **30**, L639 (1991).
[15]M. Sztucki, T. Metzger, I. Kegel, A. Tilke, D. Lubbert, J. Arthur, and J. Patel, J. Appl. Phys. **92**, 3694 (2002).
[16]J. Tersoff, Phys. Rev. B **38**, 9902 (1988).
[17]F. H. Stillinger and T. A. Weber, Phys. Rev. B **31**, 5262 (1985).
[18]N. Cherkashin, P. Calvo, F. Cristiano, B. de Mauduit, and A. Claverie, Mater. Res. Soc. Symp. Proc. **810**, C3.7 (2004).
[19]B. Colombeau, N. E. B. Cowern, F. Cristiano, P. Calvo, N. Cherkashin, Y. Lamrani, and A. Claverie, Appl. Phys. Lett. **83**, 1953 (2003).
[20]F. Cristiano *et al.*, Nucl. Instrum. Methods Phys. Res. B **216**, 46 (2004).
[21]Using the fitting of Gaussian line shapes plus a background term to all the scans over the [110] direction, we determined that the maximum is at $h = 1.243 \pm 0.003$.
[22]P. R. Bevington, *Data Reduction and Error Analysis for the Physical Sciences* (McGraw-Hill, New York, 1992).
[23]A. Claverie, B. Colombeau, B. de Mauduit, C. Bonafos, X. Hebras, G. B. Assayag, and F. Cristiano, Appl. Phys. A **76**, 1025 (2003).
[24]V. C. Venezia, R. Kalyanaraman, H.-J. L. Gossmann, C. S. Rafferty, and P. Werner, Appl. Phys. Lett. **79**, 1429 (2001).
[25]P. Partyka, Y. Zhong, K. Nordlund, R. S. Averback, I. K. Robinson, and P. Ehrhart, Phys. Rev. B **64**, 235207 (2002).